Structural Properties and Control of Soft Rods Modeled with Discrete Cosserat Rods.

Lekan Molu

***Abstract*—Soft robots featuring reduced-order and approximate finite-dimensional models are increasingly becoming paramount in literature and applications. No rigorous first-principles derivation of the structural Lagrangian properties of these soft robot models however exist, save for a few erroneous claims in literature that extend the Lagrangian properties of rigid robots to these soft systems. In this paper, we investigate the structural properties of soft robots modeled as discrete Cosserat rods by considering the components of the partial integro-diferential equation that constitute the Newton-Euler Lagrangian model. We then prescribe a few control schemes for these soft robot models. Our numerical results demonstrate consistency with our hypothesis. The results presented here are set to clarify and give a concrete proof of the results that have been erstwhile been assumed in the soft robotics community. In this paper, we consider finite-dimensional models of virtually infinite degrees-of-freedom soft robots with our focus towards establishing soft robots' dynamic properties from the ground up. The vast majority of results established in literature assume a direct correspondence from rigid robots' properties to soft robots'. However, the constituents of the stiffness tensors, mass inertia matrices, and Coriolis forces are vastly different and possess different mathematical forms in both cases. We point out and correct misleading proofs commonly cited in soft robotics literature by providing a first-principles derivation of the properties of slender soft robots under a discrete strain parameterization scheme. The proofs are then accompanied by model-based control design that validate our mathematical hypotheses on different numerical control tasks.**

Supplementary material — The codes for reproducing the experiments reported in this paper are available online: https://github.com/robotsorcerer/dcm.

I. Introduction

Soft robots, owing to their continuum strain characteristics, provide physical geometry mutability that negotiates better configurability and compliance in applications including assistive wearable devices [23, 1], robot grippers [12], confined spaces, and mobile manipulation [13]. Their inherent reconfigurability enables customizable solutions that make them preferred to rigid robots. Given their potential infinite degrees-of-freedom, soft robot control strategies have historically relied on model-free schemes. However, these techniques are not interpretable since they *mostly* employ data-driven black-box models — making model-free control only realizable via *a priori* unknown parameters. This implies an extra computational cost of running the control loop for an elongated duration before steady-state convergence is achieved.

On the contrary, a complete dynamical model of these virtually infinite degrees-of-freedom systems can be characterized by nonlinear partial differential equations (PDEs). While the theory of linear PDEs is well-developed, the theory of nonlinear PDEs is still an active research area and efforts in model-based control for *physical robots* via PDEs are very scanty. In the absence of large deformations, their dynamics can be approximated by nodal strain discretizations in the form of finite rods — mathematically characterized via ordinary differential equations (ODEs). These schemes have inspired *tractable* mathematical and approximate finite-dimensional models of soft robotic systems. Reasonably *accurate, interpretable, and robust* model-based closed-loop feedback control strategies are now feasible [7].

In this paper, we focus on robots modeled as slender, flexible rods. By physical design, these are infinite dimensional systems which require infinite partial differential equations to realize complete mathematical models and asymptotic control. Given the complexity of modeling *nonlinear* partial differential equations, we defer analysis and control in these infinite-dimensional domains to a future work. Here, we focus on discretized approximations to the nonlinear PDE systems at specific nodal points in the robot's PDE model (see Fig. 1); this provides a finite-dimensional approximation as asymptotic expansions of the infinite-dimensional259219 system. Specifically, the strain-parameterized piecewise constant strain (PCS) dynamics model of Renda et al. [16] in a reduced special Euclidean-3 group ($\mathbb{SE}(3)$) model is considered. This model addresses torsion, in-plane, and out-of-plane (multi-) bending motions with finite ordinary differential equations (ODEs) in the form of the standard Newton-Euler dynamic equations for rigid mechanical robots. In these small elastic deformations regime, soft robots can be modeled as a collection of thin and flexible slender rods where discretized linear approximations (e.g. as a special Euclidean-3 group i.e. $\mathbb{SE}(3)$) to the nonlinear system at specific nodal points (see Fig. 1) provide a finite-dimensional approximation to the infinite-dimensional system [2, 5]. An example is the recent strain-parameterized piecewise constant strain (PCS) dynamics of Renda et al. [16]. This model characterizes the motion of continuum and soft robots by considering the entire robot as a collection of discrete segments, whose dynamics is governed by standard Newton-Euler ODEs similar to the ODE characterization of rigid

The author is with Microsoft Research NYC. Email: lekan-molu@microsoft.com

mechanical robots.

The Newton-Euler characterization of the dynamics of rigid bodies has a long and studied history in rigid robotics with the skew-symmetric structural Lagrangian properties of the mass and Coriolis forces formally prescribed via Christoffel symbols in [19]. Using classical tools from Hamiltonian mechanics and Riemannian geometry, Spong [20] established symmetric properties of the Lagrangian rigid robot dynamics. The lower-boundedness of the eigenvalues of the mass matrix of rigid robots characterized by standard Newton-Euler Lagrangian dynamics was prescribed in Romero et al. [17].

Extending these properties to the finite-dimensional dynamics of soft robots is often assumed to take a direct translational correlation in the soft robotics literature. These works make fallacious assumptions on the equitability of the components that constitute the tensors in both rigid and soft robot's Newton-Euler equations. For example, Pustina et al. [15] assumed a generalized rigid manipulator mass inertia tensor and Coriolis forces in their N-E formulation. However, these tensors are composed of rigid-body masses of each link as opposed to the spatially distributed mass densities that is characteristic of soft robots' mass tensors. Even so, the Christoffel symbol employed in Coriolis forces tensors that characterizes rigid robot's dynamics ado not extend directly to soft robots' Coriolis forces. Fallacies in this regard abound in the proofs of the equivalence of the skew-symmetric mass derivative and Coriolis tensors Caasenbrood et al. [6], Pustina et al. [15]. As a result, the skew-symmetric property commonly cited from rigid robot dynamics' such as Slotine [19], Spong [20], Spong and Vidyasagar [22] does not apply to the conclusion drawn in the proofs for soft robot dynamics (such as Pustina et al. [15, Section II.C] and Caasenbrood et al. [6]) on a careful examination.

In this paper, we set out to first correct these common anomalies by giving a first-principle proof, taking models of soft robots as slender rods, and with dynamics approximated via continuously adjoined discretized nodal strains in the form of the piecewise constant strain, as a classical example. We then attempt control on the established given properties as a didactic validation of these proofs. Owing to space constraints, we defer numerical evaluation on the parameter identification proof given in Property 4 of Section III.

In this sentiment, considering the PCS model for soft multisection arms, we first establish the structural properties of their Lagrangian dynamics. We then exploit these for the steady-state convergence analyses in various control proposals (under different operating model parameters) and in different surrounding mediums using the well-established method of Lyapunov analysis. The Octopus robot [11], a muscular hydrostat [9] with distributed deformation throughout its articulated arms, blends the interplay between continuum mechanics and sensorimotor control well. Thus, we consider a single arm of the CyberOctopus [18] (configuration shown in Fig. 1) to benchmark our controllers.

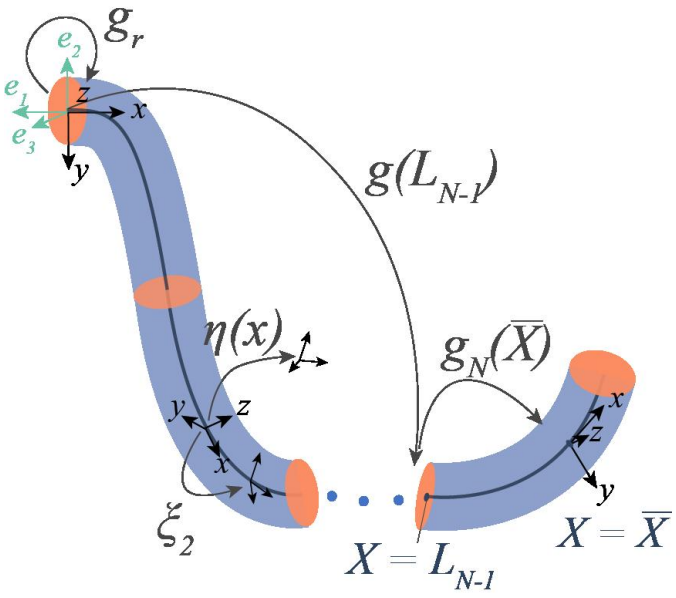

Fig. 1. Schematic of the configuration of an Octopus robot arm.

The rest of this paper is structured as follows: in §II, we briefly introduce preliminaries relevant to the contributions machinery we present in §III. Multivariable stabilizing feedback controllers for regulating the tip point and strain states are established in §IV. We present numerical results in §V and conclude the paper in §VI.

II. Notations and Preliminaries

The strain field and strain twist vectors are respectively $\xi \in \mathbb{R}^6$ and $\eta \in \mathbb{R}^6$. The Lie algebra of $\mathbb{SE}(3)$ is $\mathfrak{se}(3)$. All rotation are measured counterclockwise in corkscrew sense. The continuum is reduced to a space curve defined by a material abscissa $X : [0, L]$, where L is the robot's length in the reference configuration. For a configuration $\boldsymbol{g}(X) \in \mathbb{SE}(3)$, its adjoint and coadjoint representations are respectively $\mathrm{Ad}_{\boldsymbol{g}}$, $\mathrm{Ad}^{\star}_{\boldsymbol{g}}$ — parameterized by a curve, the material abscissa X. The corresponding adjoint and coadjoint representation of the strain twist vector are $\mathrm{ad}_{\xi,\eta}$ and $\mathrm{ad}^{\star}_{\xi,\eta}$, respectively. In generalized coordinate, the joint vector of a soft robot is denoted $q(\xi) = [\xi_1^{\top}, \ldots, \xi_{n_\xi}^{\top}]^{\top} \in \mathbb{R}^{6n_\xi}$.

A. SoRo Configuration

The inertial frame is signified by the basis triad $(\boldsymbol{e}_1, \boldsymbol{e}_2, \boldsymbol{e}_3)$ (see Fig. 1) and $\boldsymbol{g}_r(X)$ is the transformation from the inertial to the manipulator's base frame. For cable-driven arms, the point at which actuation occurs is labeled $\bar{X}$. The configuration matrix that parameterizes curve X of length L_n is denoted $\boldsymbol{g}_{L_n}$. The cable runs through the z-axis in the (micro) body frame (x-axis in the spatial frame). As shown in Fig. 1, the transformation from the base to the

inertial frame is

$$\boldsymbol{g}_r = \begin{pmatrix} 0 & -1 & 0 & 0 \\ 1 & 0 & 0 & 0 \\ 0 & 0 & 1 & 0 \\ 0 & 0 & 0 & 1 \end{pmatrix}. \tag{1}$$

We adopt a linear viscoelastic constitutive model based on Kelvin-Voight internal forces i.e.

$$\mathcal{F}_i(X) = \Sigma(\xi - \xi_0) + \Upsilon\dot{\xi}, \tag{2}$$

with Σ being the constant screw stiffness matrix, Υ the viscosity matrix, and the reference strain $\xi_0 = [0, 0, 0, 1, 0, 0]^\top$ in the upright configuration. The jacobian associated with X is $J(X)$. Owing to paper length constraints we refer readers to Renda et al. [16] for further definitions.

B. Continuous Strain Vector and Twist Velocity Fields

Let $p(X)$ describe the position vector of a microsolid on a soft body and let $R(X)$ denote the corresponding orientation matrix. Furthermore, let the pose $[p(X), R(X)]$ be parameterized by a material abscissa $X \in [0, L]$ for end nodes 0 and L. Then, the robot's C-space, parameterized by a curve $g(X) : X \to \mathbb{SE}(3)$, is $g(X) = \begin{pmatrix} R(X) & p(X) \\ 0^\top & 1 \end{pmatrix}$. Suppose that $\varepsilon(X) \in \mathbb{R}^3$ and $\gamma(X) \in \mathbb{R}^3$ respectively denote the linear and angular strain components of the soft arm. Then, the arm's strain field is a state vector along the curve $g(X)$ defined as $\check{\xi}(X) = g^{-1}\partial g/\partial X \triangleq g^{-1}\partial_x g$, and the velocity of $g(X)$ is the twist vector field $\check{\eta}(X)$ defined as $\check{\eta}(X) = g^{-1}\partial g/\partial t \triangleq g^{-1}\partial_t g$. Read $\hat{\gamma}$: the anti-symmetric matrix representation of γ. Read $\check{\xi}$: the isomorphism from $\xi \in \mathbb{R}^6$, to its matrix representation in $\mathfrak{se}(3)$.

C. Discrete Cosserat System: Cosserat-Constitutive PDEs

The PCS model assumes that the respective strain, ξ_i for n microsolid sections, $\{\mathcal{M}_i\}_{i=1}^n$, are constant for each discretized section of the arm. Using d'Alembert's principle, the generalized dynamics for the PCS model (cf. Fig. 1) under external and actuation loads admits the weak form [16]

$$\begin{aligned} &\underbrace{\left[\int_0^{L_N} J^T \mathcal{M}_a J dX\right]}_{M(q)} \ddot{q} + \underbrace{\left[\int_0^{L_N} J^T \mathrm{ad}^\star_{J\dot{q}} \mathcal{M}_a J dX\right]}_{C_1(q,\dot{q})} \dot{q} + \\ &\underbrace{\left[\int_0^{L_N} J^T \mathcal{M}_a \dot{J} dX\right]}_{C_2(q,\dot{q})} \dot{q} + \underbrace{\left[\int_0^{L_N} J^T \mathcal{D} J \|J\dot{q}\|_p dX\right]}_{D(q,\dot{q})} \dot{q} \\ &- \underbrace{(1 - \rho_f/\rho)\left[\int_0^{L_N} J^T \mathcal{M} \mathrm{Ad}^{-1}_{\boldsymbol{g}} dX\right]}_{N(q)} \mathrm{Ad}^{-1}_{\boldsymbol{g}_r}\mathcal{G} - \underbrace{J(\bar{X})^T \mathcal{F}_p}_{F(q)} \\ &- \underbrace{\int_0^{L_N} J^T \left[\nabla_x \mathcal{F}_i - \nabla_x \mathcal{F}_a + \mathrm{ad}^\star_{\eta_n}(\mathcal{F}_i - \mathcal{F}_a)\right] dX}_{\tau(q)} = 0, \end{aligned} \tag{3}$$

where $\mathcal{F}_i(X) \triangleq \left(M_i^T, F_i^T\right)^T \equiv \partial_X \mathfrak{U}$ is the wrench of internal forces, $\bar{\mathcal{F}}_a(X)$ is the *distributed* wrench of actuation loads, and $\bar{\mathcal{F}}_e(X)$ is the external *distributed* wrench of the applied forces. The screw mass inertia matrix $\mathcal{M}(X) = \mathrm{diag}\,(I_x, I_y, I_z, A, A, A)\,\rho$ for a body density ρ, sectional area A, bending, torsion, and second inertia operator I_x, I_y, I_z respectively. In (3), $\mathcal{M}_a = \mathcal{M} + \mathcal{M}_f$ is a lumped sum of the microsolid mass inertia operator, $\mathcal{M}$, and that of the added mass fluid, $\mathcal{M}_f$; dX is the length of each section of the multi-robot arm; $\mathcal{D}(X)$ is the drag matrix; $J(X)$ is the Jacobian operator; $\|\cdot\|_p$ is the translation norm of the expression contained therein; ρ_f is the density of the fluid in which the material moves; ρ is the body density; $\mathcal{G} = [0, 0, 0, -9.81, 0, 0]^T$ is the gravitational vector; and $\mathcal{F}_p$ is the applied wrench at $\bar{X}$. In standard Newton-Euler form, equation (3), is

$$\begin{aligned} M(q)\ddot{q} + [C_1(q,\dot{q}) + C_2(q,\dot{q})]\,\dot{q} = \tau(q) + F(q) \\ + N(q)\mathrm{Ad}^{-1}_{\boldsymbol{g}_r}\mathcal{G} - D(q,\dot{q})\dot{q}. \end{aligned} \tag{4}$$

III. Properties of Soft Robot Dynamics

In this section, we carefully derive the properties of the Newton-Euler dynamics of soft robots characterized as finite-dimensional discrete Cosserat ODE models. We now establish the Lagrangian properties.

Theorem 1 (The kinetic equation)**.** *Equation* (4) *satisfies the following properties:*

Property 1 (Positive definiteness of the Inertia Operator)**.** *The inertia tensor $\mathcal{M}_a(q)$ is symmetric and positive definite. As a result $M(q)$ is symmetric and positive definite.*

Proof of Property 1. The jacobian, J, is injective by [16, equation 20]. Thus, property 1 follows from its definition. □

Property 2 (Boundedness of the Mass Matrix)**.** *The mass inertial matrix $M(q)$ is uniformly bounded from below by $m\boldsymbol{I}_n$ where m is a positive constant.*

Proof of Property 2. This is a restatement of the lower boundedness of $M(q)$ for fully actuated n-degrees of freedom manipulators [17]. □

Property 3 (Skew symmetric property)**.** *The matrix $\dot{M}(q) - 2\,[C_1(q,\dot{q}) + C_2(q,\dot{q})]$ is skew-symmetric.*

Proof of Property 3. We have by Leibniz's rule that

$$\begin{aligned} \dot{M}(q) &= \frac{d}{dt}\left(\int_0^{L_N} J^T \mathcal{M}_a J dX\right) = \int_0^{L_N} \frac{\partial}{\partial t}\left(J^T \mathcal{M}_a J\right) dX \\ &\triangleq \int_0^{L_N} \left(\dot{J}^T \mathcal{M}_a J + J^T \dot{\mathcal{M}}_a J + J^T \mathcal{M}_a \dot{J}\right) dX. \end{aligned} \tag{5}$$

Therefore, $\dot{M}(q) - 2\left[C_1(q,\dot{q}) + C_2(q,\dot{q})\right]$ becomes

$$\int_0^{L_N} \left(\dot{J}^\top \mathcal{M}_a J + J^\top \dot{\mathcal{M}}_a J + J^\top \mathcal{M}_a \dot{J}\right) dX$$
$$- 2\int_0^{L_N} \left(J^\top \mathrm{ad}^\star_{J\dot{q}} \mathcal{M}_a J + J^\top \mathcal{M}_a \dot{J}\right) dX \tag{6}$$
$$\triangleq \int_0^{L_N} \left(\dot{J}^\top \mathcal{M}_a J + J^\top \dot{\mathcal{M}}_a J - J^\top \mathcal{M}_a \dot{J}\right) dX$$
$$- 2\int_0^{L_N} J^\top \mathrm{ad}^\star_{J\dot{q}} \mathcal{M}_a J dX. \tag{7}$$

Similarly, $-\left[\dot{M}(q) - 2\left[C_1(q,\dot{q}) + C_2(q,\dot{q})\right]\right]^\top$ expands as

$$-\dot{M}^\top(q) + 2\left[C_1^\top(q,\dot{q}) + C_2^\top(q,\dot{q})\right] =$$
$$\int_0^{L_N} dX^\top \left(-J^\top \mathcal{M}_a \dot{J} - J^\top \dot{\mathcal{M}}_a J - \dot{J}^\top \mathcal{M}_a J\right)$$
$$+ 2\int_0^{L_N} dX^\top \left(J^\top \mathcal{M}_a \mathrm{ad}_{J\dot{q}} J + \dot{J}^\top \mathcal{M}_a J\right)$$
$$\triangleq \int_0^{L_N} \left(J^\top \mathcal{M}_a \dot{J} - \dot{J}^\top \mathcal{M}_a J - J^\top \dot{\mathcal{M}}_a J\right) dX$$
$$- 2\int_0^{L_N} J^\top \mathrm{ad}^\star_{J\dot{q}} \mathcal{M}_a J dX \tag{8}$$

where the terms in equation (8) follow from the symmetry of the matrices that constitute the integrands. Inspecting (7) and (8), it is easy to see that their right hand sides verify the identity

$$\int_0^{L_N} \left(\dot{J}^\top \mathcal{M}_a J + J^\top \dot{\mathcal{M}}_a J - J^\top \mathcal{M}_a \dot{J}\right) dX$$
$$- 2\int_0^{L_N} J^\top \mathrm{ad}^\star_{J\dot{q}} \mathcal{M}_a J dX = 2\int_0^{L_N} J^\top \mathrm{ad}^\star_{J\dot{q}} \mathcal{M}_a J dX -$$
$$\int_0^{L_N} \left(J^\top \mathcal{M}_a \dot{J} - \dot{J}^\top \mathcal{M}_a J - J^\top \dot{\mathcal{M}}_a J\right) dX \tag{9}$$

or

$$\dot{M}(q) - 2\left[C_1(q,\dot{q}) + C_2(q,\dot{q})\right] =$$
$$-\left[\dot{M}(q) - 2\left[C_1(q,\dot{q}) + C_2(q,\dot{q})\right]\right]^\top. \tag{10}$$

A fortiori, the skew symmetric property follows. □

Remark 1. *Since $\dot{M}(q)$ is symmetric (cref. (5)), another way of stating the skew-symmetric property is to write*

$$\dot{M}(q) = C_1(q,\dot{q}) + C_2(q,\dot{q}) + \left[C_1(q,\dot{q}) + C_2(q,\dot{q})\right]^\top. \tag{11}$$

Owing to the symmetry of the right-hand-side (rhs), we have $\dot{M} = 2(C_1 + C_2)$.

Property 4 (Linearity-in-the-parameters)**.** *There exists a constant vector $\Theta \in \mathbb{R}^l$ and an $N \times l$ dimensional regressor function $Y(q,\dot{q},\ddot{q}) \in \mathbb{R}^{N\times l}$ such that*

$$M(q)\ddot{q} + \left[C_1(q,\dot{q}) + C_2(q,\dot{q}) + D(q,\dot{q})\right]\dot{q} - F(q) -$$
$$+ N(q) Ad^{-1}_{\boldsymbol{g}_r} \mathcal{G} = Y(q,\dot{q},\ddot{q})\Theta. \tag{12}$$

Proof of Property 4. Consider the generalized constitutive law for the full Cosserat model derived in [3, §6.3]. The reduced Lagrangian density in $\mathfrak{se}(3)$ per unit of deformed volume (for all configurations)[1] for a configuration $\mathcal{B}$ is $\mathfrak{L} = \mathfrak{T} - \mathfrak{U}$ [3] where $\mathfrak{T}, \mathfrak{U}$ respectively denote the volume's left-reduced kinetic and elastic potential energy densities in $\mathcal{B}$. From the Euler-Lagrange equation, we have

$$\tau_n = \frac{d}{dt}\frac{\partial \mathfrak{T}}{\partial \dot{\xi}_n} - \frac{\partial \mathfrak{T}}{\partial \xi_n} + \frac{\partial \mathfrak{U}}{\partial \eta_n}, \quad n = 1,\ldots,N. \tag{13}$$

Suppose that the material mid-surface crosses the microstructures $\mathcal{M}_i$ which correspond to the mass center, then the kinetic energy density per unit of deformed area and its rate of change w.r.t ξ are [3]

$$\mathfrak{T}(\xi) = \frac{1}{2}\left\langle \begin{pmatrix} \omega \\ \nu, \end{pmatrix}, \begin{pmatrix} \bar{I}\omega \\ \bar{\rho}\nu \end{pmatrix} \right\rangle \tag{14}$$
$$\mathfrak{T}(\dot{\xi}) = \frac{1}{2}\left\langle \begin{pmatrix} \dot{\omega} \\ \dot{\nu}, \end{pmatrix}, \begin{pmatrix} \bar{I}\dot{\omega} \\ \bar{\rho}\dot{\nu} \end{pmatrix} \right\rangle \tag{15}$$

where $\bar{\rho}$ and $\bar{I}$ respectively denote the mass and angular inertia density per unit volume. It follows that

$$\partial_\xi \mathfrak{T} = \begin{pmatrix} \bar{I}\omega \\ \bar{\rho}\nu \end{pmatrix}, \quad \partial_{\dot{\xi}} \mathfrak{T} = \begin{pmatrix} \bar{I}\dot{\omega} \\ \bar{\rho}\dot{\nu} \end{pmatrix}. \tag{16}$$

In a similar vein, the left invariant density of internal energy $\mathfrak{U}$ is [4]

$$\mathfrak{U}(\eta) = \langle \mathcal{F}_{int}, (\eta - \eta^d) \rangle \tag{17}$$

for a desired η^d and field of internal force constraints $\mathcal{F}_{int} : X \in [0,L] \to \mathcal{F}_{int}(X) \in \mathfrak{se}(3)$. The potential energy per unit of metric area of the deformed surface (assuming that it is concentrated in the mid-surface) is [3]

$$\partial_\eta \mathfrak{U} = \begin{pmatrix} \partial\mathfrak{U}/\partial\gamma \\ \partial\mathfrak{U}/\partial\varepsilon \end{pmatrix} - \begin{pmatrix} 0 \\ \varepsilon \end{pmatrix} \mathfrak{L} \tag{18}$$

so that the Euler-Lagrange equation (13) becomes

$$\begin{pmatrix} \bar{I}\ddot{\omega} + \dot{\bar{I}}\dot{\omega} \\ \bar{\rho}\ddot{\nu} + \dot{\bar{\rho}}\dot{\nu} \end{pmatrix} - \begin{pmatrix} \bar{I}\omega \\ \bar{\rho}\nu \end{pmatrix} + \begin{pmatrix} \partial\mathfrak{U}/\partial\gamma \\ \partial\mathfrak{U}/\partial\varepsilon \end{pmatrix} - \begin{pmatrix} 0 \\ \varepsilon \end{pmatrix} \mathfrak{L}. \tag{19}$$

Observe: Under the PCS assumption, each microsolid is fixed so that the energy density per unit section of metric volume is akin to that of a rigid body. The kinetic and potential energies for the PCS model per section i of N sections becomes

$$\mathfrak{T} = \frac{1}{2}\sum_{i=1}^{N} \left\langle \begin{pmatrix} {}^{i+1}\omega_i \\ {}^{i+1}\nu_i, \end{pmatrix}, \begin{pmatrix} {}^{i+1}\bar{I}_i\, {}^{i+1}\omega_i \\ {}^{i+1}\bar{\rho}_i\, {}^{i+1}\nu_i \end{pmatrix} \right\rangle \tag{20}$$

where ${}^{i+1}\omega_i$ is the angular velocity of section $i+1$ in the frame of section i, ${}^{i+1}\nu_i$ is the linear velocity of section

[1] Note that the full Lagrangian density of the soft multisection manipulator is $L_m = \int_0^L \mathfrak{L}(\boldsymbol{g},\eta,\xi)dX$.

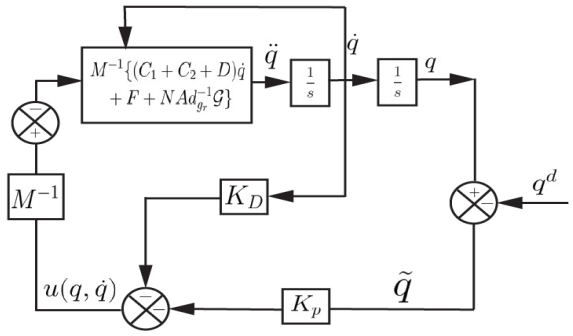

Fig. 2. PD computed torque control block diagram.

$i+1$ in the frame of section i e.t.c. Similarly, the sectional potential energies are

$$\mathfrak{U}(\eta_i) = \sum_{i=1}^{N} \langle \{\mathcal{F}_{int}\}_i, (\eta_i - \eta_i^d) \rangle. \tag{21}$$

Thus, the kinetic and potential energy are each linear in configuration parameters so that

$$\begin{aligned} \mathfrak{T} &= \sum_{i=1}^{N} \frac{\partial \mathfrak{T}}{\partial \Sigma_i} \Sigma_i = \sum_{i=1}^{N} \Gamma\mathfrak{T}_i \Sigma_i, \\ \mathfrak{U} &= \sum_{i=1}^{N} \frac{\partial \mathfrak{U}}{\partial \Sigma_i} \Sigma_i = \sum_{i=1}^{N} \Gamma\mathfrak{U}_i \Sigma_i \end{aligned} \tag{22}$$

where Σ_i is an inertial parameter, $\Gamma\mathfrak{T}_i$ is a function of $q, \dot{q}$ and $\Gamma\mathfrak{U}_i$ is a function of q. Using (22) and plugging (16) and (18) into (13), we conclude that the sectionalized piecewise Cosserat dynamics is also linear-in-the-inertial-parameters, given as $\tau(q) = Y(q, \dot{q}, \ddot{q})\Theta$, where $Y(q, \dot{q}, \ddot{q})$ is the matrix function of $q, \dot{q}, \ddot{q}$ and Θ is the matrix of parameters. □

IV. Multivariable Control

We describe the feedback control schemes which steer an arbitrary point in the joint space, $q(t)$ at time t, to a target point $q^d = (q_1^d, \ldots, q_N^d)^\top$[2] underwater and in terrestrial-operated environments. The position $q(t)$ is asymptotically stable from a systematic viewpoint if the potential function has a minimum at $q(t) = q^d$ for a desired equilibrium strain state $q^d(t)$. We will control the robot's dynamics by exploiting the properties of §III. The general structure of the control scheme is illustrated in Fig. 2.

A. Proportional-(Integral)-Derivative Control, Redux.

We first show that regarding the generalized torque $\tau(q)$ as a control input, $u(q, \dot{q})$, linear feedback laws are (almost) sufficient for attaining a desired joint configuration (without gravity compensation) in the control law.

Theorem 2 (Cable-driven Actuation)**.** *For a set of gains K_D and K_p which are damping and positive diagonal matrices, the control law (without gravity/buoyancy compensation)*

$$u(q, \dot{q}) = -K_p\tilde{q} - K_D\dot{q} - F(q) \tag{23}$$

under a cable-driven actuation globally asymptotically stabilizes (GAS) system (4), where $\tilde{q}(t) = q(t) - q^d$ is the joint error vector for a desired equilibrium point in space q^d.

Proof. Without gravity, the term $N(q)\mathrm{Ad}_{g_r}^{-1}\mathcal{G} = 0$. Let

$$\breve{C}(q, \dot{q}) = C_1(q, \dot{q}) + C_2(q, \dot{q})$$

and write (4) for an arbitrary control input $u(q)$ as

$$M(q)\ddot{q} = u(q, \dot{q}) + F(q) - \left[\breve{C}(q, \dot{q}) + D(q, \dot{q})\right]\dot{q}. \tag{24}$$

Consider the Lyapunov candidate function

$$V(q) = \frac{1}{2}\dot{q}^\top M(q)\dot{q} + \frac{1}{2}\tilde{q}^\top K_p\tilde{q}. \tag{25}$$

Observe: $V(q) > 0 \; \forall \; \{q, q^d\} \setminus (q = q^d), \dot{q} \neq 0$; and $V(q) = 0 \; \forall \{q, q^d\}$ when $(q = q^d)$ and $\dot{q} = 0$ in the joint space. Differentiating $V(q)$ yields

$$\begin{aligned} \dot{V}(q) &= \dot{q}^\top M(q)\ddot{q} + \frac{1}{2}\dot{q}^\top \dot{M}(q)\dot{q} + \tilde{q}^\top K_p\dot{\tilde{q}}, \\ &= \dot{q}^\top \left(u(q, \dot{q}) + F(q) - \left[\breve{C}(q, \dot{q}) + D(q, \dot{q})\right]\dot{q}\right) \\ &\quad + \frac{1}{2}\dot{q}^\top \dot{M}(q)\dot{q} + \tilde{q}^\top K_p\dot{q}, \\ &= \dot{q}^\top \left(u(q, \dot{q}) + F(q) - \left[\breve{C}(q, \dot{q}) + D(q, \dot{q})\right]\dot{q}\right) \\ &+ \tilde{q}^\top K_p\dot{q} + \dot{q}^\top \left[\frac{1}{2}\left(\dot{M}(q) - 2\breve{C}(q, \dot{q})\right) + \breve{C}(q, \dot{q})\right]\dot{q}, \\ &= \dot{q}^\top \left[u(q, \dot{q}) + F(q) + K_p\tilde{q} - D(q, \dot{q})\dot{q}\right] \end{aligned} \tag{26}$$

where the last line follows from the skew symmetric property established in Remark 1. Suppose we choose the control law (23), then

$$\dot{V}(q) = -\dot{q}^\top \left[K_D + D(q, \dot{q})\right]\dot{q} \leq 0 \tag{27}$$

if we choose K_D as a block diagonal matrix of positive gains since the drag term $D(q, \dot{q}) > 0$. Thus, we have that the potential function is decreasing if q is non-zero. However, asymptotic stability of trajectories as a result of the potential (Lyapunov) function candidate does not automatically follow since $\dot{V}(t)$ is not negative at $\dot{q} = 0$. That is, it is possible for the manipulator's joint space variable derivative $\dot{q} = 0$ when $q \neq q^d$.

To prove global asymptotic stability, suppose the domain $\Omega \subset D \in \mathbb{R}^{6N \times 6N}$ is the compact, positively invariant domain with respect to (4). Let $\mathcal{E}$ be the set of all $q \in \Omega$ where $\dot{V}$ is identically zero so that (27) implies that $\dot{q} = 0$ and $\ddot{q} = 0$. From (24), we must have

$$M(q)\ddot{q} + \left[\breve{C}(q, \dot{q}) + D(q, \dot{q})\right]\dot{q} = -K_p\tilde{q} - K_D\dot{q} \tag{28}$$

which implies that $0 = -K_p\tilde{q}$ and hence $\tilde{q} = 0$. If Υ is the largest invariant set of $\mathcal{E}$, then by LaSalle's invariance theorem [10], every solution starting in Ω approaches Υ as $t \to \infty$. Whence, the equilibrium is GAS. □

Corollary 1 (Fluid-driven actuation)**.** *If the robot is operated without cables, and is driven with a dense medium such as*

[2]Here, q_i is the joint space for a section of the multisection manipulator.

pressurized air or water, then the term $F(q) = 0$ so that the control law

$$u(q, \dot{q}) = -K_p \tilde{q} - K_D \dot{q} \tag{29}$$

globally asymptotically stabilizes the system.

Proof. The proof follows easily since $F(q) = 0$ in (26). □

Theorem 3 (Gravity/Buoyancy-Compensated Control)**.** *Without gravity and/or buoyancy-compensation, there are parasitic disturbances and unmodeled parameters in (4) where an offset in the positional error $\tilde{q}$ at steady state may show up since we do not explicitly compensate for gravity and buoyancy.where the PD control law is not sufficient for driving the strain states to equilibrium. The following controller will achieve zero steady state convergence.*

$$u(q, \dot{q}) = -K_p \tilde{q} - K_D \dot{q} - F(q) - N(q) Ad_{g_r}^{-1} \mathcal{G}. \tag{30}$$

Proof. From (4), write

$$\begin{aligned} M(q)\ddot{q} = u(q, \dot{q}) + F(q) + N(q)\mathrm{Ad}_{g_r}^{-1}\mathcal{G} \\ - \left[\breve{C}(q, \dot{q}) + D(q, \dot{q})\right] \dot{q}. \end{aligned} \tag{31}$$

Let us choose the Lyapunov function candidate

$$V(q) = \frac{1}{2}\dot{q}^\top M(q)\dot{q} + \frac{1}{2}\tilde{q}^\top K_p \tilde{q} + \frac{1}{2}\int_0^t \tilde{q}^\top(s) K_I \tilde{q} ds, \tag{32}$$

where $V(q) > 0 \; \forall \; \{q, q^d\} \setminus (q = q^d), \dot{q} \neq 0$; $V(q) = 0 \; \forall \{q, q^d\}$ when $(q = q^d)$, K_I is the block diagonal integral gain, and $\dot{q} = 0$ in the joint space. Tt can be verified that

$$\begin{aligned} \dot{V}(q) = \dot{q}^\top \Bigg[u(q, \dot{q}) + F(q) + \left\{ K_p + \frac{K_I}{s} \right\} \tilde{q} \\ - D(q, \dot{q})\dot{q} + N(q)\mathrm{Ad}_{g_r}^{-1}\mathcal{G} \Bigg] \end{aligned} \tag{33}$$

where we have used the frequency domain representation of the integral operator i.e. $1/s$. If we set

$$u(q, \dot{q}) = -\left\{ K_p + \frac{K_I}{s} \right\} \tilde{q} - K_D \dot{q} - F(q) - N(q)\mathrm{Ad}_{g_r}^{-1}\mathcal{G}, \tag{34}$$

we must have

$$\dot{V}(t) = -\dot{q}^\top \left[K_D + D(q, \dot{q}) \right] q \leq 0, \text{ if } \dot{q} \neq 0 \tag{35}$$

else for $\dot{V}$ identically zero, LaSalle's principle applies. □

Suppose that we choose appropriate proportional and derivative gains with the gravity-compensation term in (34), then the integral again K_I may be ignored as

$$u(q, \dot{q}) = -K_p \tilde{q} - K_D \dot{q} - F(q) - N(q)\mathrm{Ad}_{g_r}^{-1}\mathcal{G}. \tag{36}$$

The proof of the theorem follows as a result.

V. Numerical Setup and Results

Our goal is to regulate the strain and strain velocity states of the robot per section under different constant tip loads *despite the inevitable non-constant loads due to gravity, external forces, and inertial forces*.

A. System Setup and Parameters

As seen in Fig. 1, the tip load acts on the $+y$-axis in the robot's base frame. We use $\mathcal{F}_p^y$ to represent the tip load acting along the $+y$ direction in what follows. Given the geometry of the robot, we choose a drag coefficient of 0.82 (a Reynolds number of order 104) for underwater operations. We set the Young's modulus, $E = 110kPa$ and the shear viscosity modulus to $3kPa$. The bending second inertia momenta are set to $I_y = I_z = \pi r^4/4$ while the torsion second moment of inertia is set to $I_x = \pi r^4/2$ for $r = 0.1m$, the arm's radius – uniform across sections. The arm length is $L = 0.2m$. We assume a (near-incompressible) rubber material makes up the robot's body and set its Poisson ratio to 0.45; the mass is chosen as $\mathcal{M} = \rho[I_x, I_y, I_z, A, A, A]$ for a cylindrical soft shell's nominal density of $\rho = 2,000kgm^{-3}$ as used in [16]; the cross-sectional area $A = \pi r^2$ so that $I_x = \pi r^4/2$. The drag screw stiffness matrix D in (4) is a function of each section's geometry and hydrodynamics so that $D = -\rho_w \nu^T \nu \breve{D} \nu/|\nu|$ where ρ_w is the water density set to $997kg/m^3$, and $\breve{D}$ is the tensor that models the geometry and hydrodynamics factors in the viscosity model (see [16, §II.B, eq. 6]). The curvilinear abscissa, $X \in [0, L]$ was discretized into 41 microsolids per section.

B. Discussion

We adopted the recursive articulated-body algorithm [8] and integrate the right-hand-side of differential equations (24) and (31) using a Runge-Kutta-Fehlberg (RKF) adaptive scheme implemented in Python and Torch [14] with relative and absolute errors respectively set to 10^{-7} and 10^{-9}. We have found these tolerance values to be crucial for a successful numerical integration scheme as it avoids numerical instability. Depicted on the vertical axes of each chart of Fig. 3 are the strain positions or twists along $+y$-direction (on the robot's local frame) while the horizontal axes depict the number of adaptive RKF (re-) integration steps per for every tenth of a second. The trajectory evolution over time per discretized Cosserat section is shown in the various "dash-dotted" lines, while the "solid blue" lines denote the reference. The controller parameters are annotated within chart together with the amount of constant tip load in Newtons. We see that all joint configurations are stabilized to reference strain twist states ($\dot{q}^d$) for respective constant tip loads. It can also be inferred that more sections a in the discretized Cosserat model lead to less bumpy state regulation strategy.

In (*a1–a3*), the strain twists are precisely regulated to zero offset errors despite large constant tip loads (*a1-a3*); and with small tip disturbances *(a4)*. Notably, the large value of the proportional gain causes overdamping in the transients before convergence. However, a 20% error offset at steady state is observed in the linear strain position regulation case **(b1)** in the absence of the gravity compensation term in the control law. We attribute this to the nature of PD Lagrangian controllers realized via computed torque methods [21]. For

a1) Cable-driven, strain twist setpoint terrestrial control.

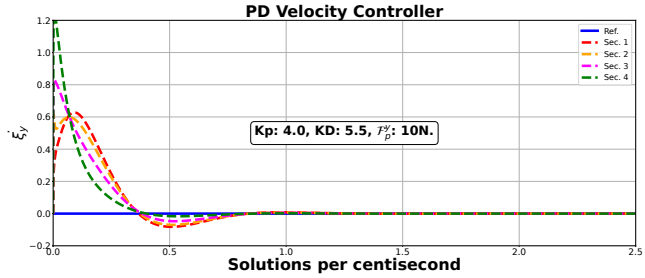

a2) Fluid-actuated, strain twist setpoint terrestrial control.

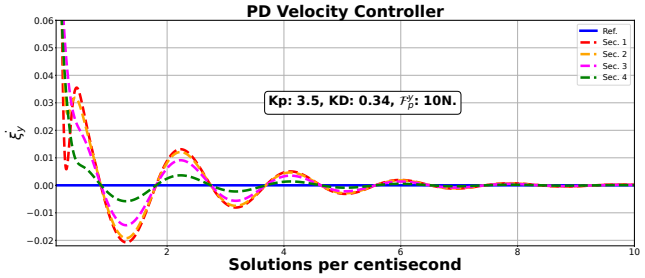

a3) Fluid-actuated, strain twist setpoint underwater control.

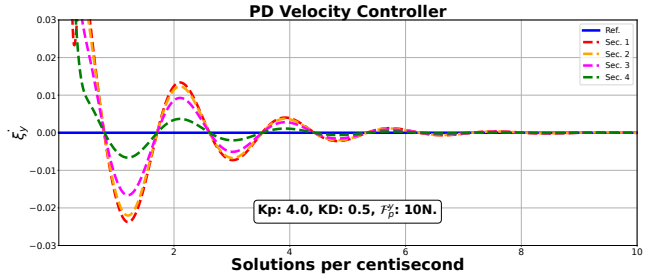

a4) Cable-driven, strain twist setpoint regulation.

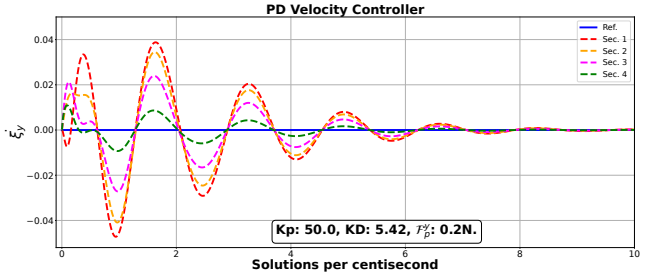

b1) Position control with no gravity-compensation.

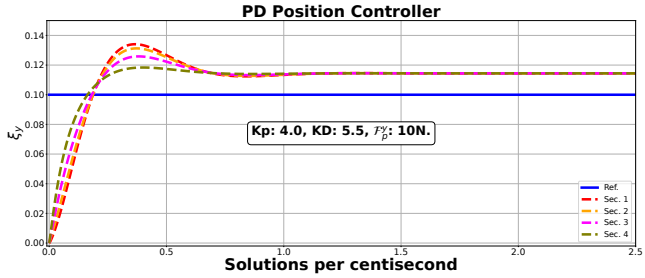

b2) Gravity-compensated terrestrial position control.

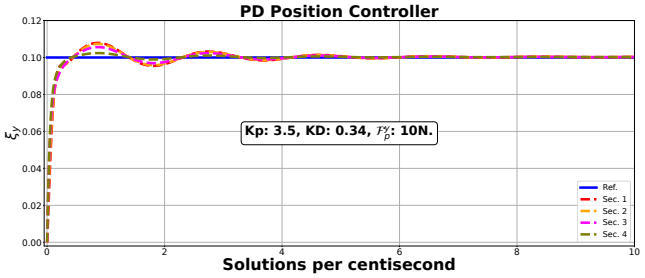

Fig. 3. *(a1 – a3):* Linear strain twist state regulation for a 4-section (41 microsolid pieces per section) soft arm under a $10N$ lateral tip load, $\mathcal{F}_p^y$ that is *(a1)* cable-driven in a sparse medium *(a2)* fluid-actuated in a sparse medium. *(a3)* fluid-actuated in a dense medium such as water (i.e. with drag forces compensation). *(a4)* Under a miniature tip-load of $0.2N$, a cable-driven 4-section arm finely regulates strain twists to equilibrium over time. *(b1-b2)*: Linear strain position regulation for a cable-driven arm operating in air *(b1)* and a fluid-actuated arm illustrating the effect of steady state errors in the absence of gravity compensation. The horizontal axes show the number of (re)-integration time-steps per second for the adaptive Runge-Kutta-Fehlberg integrator we utilized in computing the controllers.

accurate position control with PD controllers, steady state errors can be achieved when the gravity os compensated in the control design as *(b2)* shows.

VI. Conclusion

We have presented the Lagrangian properties for soft robots under a discrete Cosserat model. These properties were then exploited to cancel out nonlinearities in the derived controllers for strain states regulation. Our numerical experiments confirm the conclusions from our Lyapunov analyses. Similar to rigid robots under PD control laws with Lagrangian dynamics, we have observed strain position steady state offsets. Position control efficacy are shown to improve if gravity and/or buoyancy is compensated in the control law.

VII. Acknowledgment

For her kind remarks, constructive criticism, and evaluative feedback, the author thanks Audrey Sedal of McGill University. To Shaoru Chen, for helping with code organization and troubleshooting for the numerical results presented in this paper, the author expresses his gratitude. A vote of thanks to James Forbes of McGill University for early manuscript feedback.

References

[1] Gunjan Agarwal, Nicolas Besuchet, Basile Audergon, and Jamie Paik. Stretchable Materials for Robust Soft Actuators Towards Assistive Wearable Devices. *Scientific reports*, 6(1):34224, 2016. 1

[2] Frederic Boyer and Federico Renda. Poincaré's equations for cosserat media: application to shells. *Journal of Nonlinear Science*, 2016.

[3] Frederic Boyer and Federico Renda. Poincaré's Equations for Cosserat Media: Application to Shells. *Journal of Nonlinear Science*, 27(1):1–44, 2017. ISSN 14321467. 4

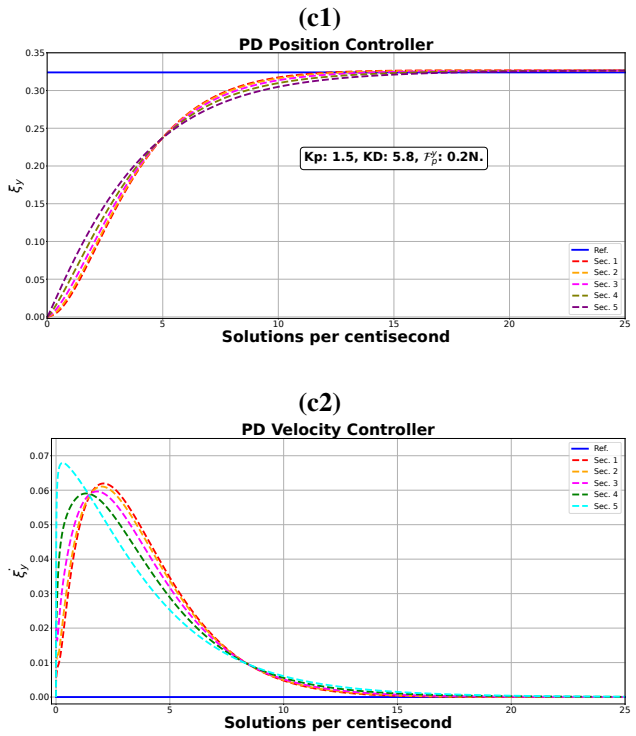

Fig. 4. Gravity-based compensation position and velocity control: **c1)** Cable-driven gravity-compensated position control. **c2)** Cable-driven gravity-compensated velocity control.

[4] Frederic Boyer, Mathieu Porez, and Alban Leroyer. Poincaré–cosserat equations for the lighthill three-dimensional large amplitude elongated body theory: application to robotics. *Journal of Nonlinear Science*, 20:47–79, 2010. 4

[5] Frédéric Boyer, Vincent Lebastard, Fabien Candelier, Federico Renda, and Mazen Alamir. Statics and Dynamics of Continuum Robots based on Cosserat Rods and Optimal Control Theories. *IEEE Transactions on Robotics*, 39(2):1544–1562, 2022. 1

[6] Brandon Caasenbrood, Alexander Pogromsky, and Henk Nijmeijer. Energy-shaping controllers for soft robot manipulators through port-hamiltonian cosserat models. *SN Computer Science*, 3(6):494, 2022.

[7] Cosimo Della Santina, Christian Duriez, and Daniela Rus. Model-based control of soft robots: A survey of the state of the art and open challenges. *IEEE Control Systems Magazine*, 43(3):30–65, 2023.

[8] Roy Featherstone. *Rigid Body Dynamics Algorithms*. Springer, 2014. 6

[9] Helmut Hauser, Rudolf M. Füchslin, and Rolf Pfeifer, editors. *Opinions and Outlooks on Morphological Computation*. Hauser, Helmut and Füchslin, Rudolf M. and Pfeifer, Rolf, 2014. ISBN 978-3-033-04515-6. 2

[10] Hassan K Khalil. *Nonlinear Control*, volume 406. Pearson New York, 2015. 5

[11] Cecilia Laschi, Matteo Cianchetti, Barbara Mazzolai, Laura Margheri, Maurizio Follador, and Paolo Dario. Soft robot arm inspired by the octopus. *Advanced robotics*, 26(7):709–727, 2012. 2

[12] Mariangela Manti, Taimoor Hassan, Giovanni Passetti, Nicolò D'Elia, Cecilia Laschi, and Matteo Cianchetti. A Bioinspired Soft Robotic Gripper for Adaptable and Effective Grasping. *Soft Robotics*, 2(3):107–116, 2015. 1

[13] Andrew D Marchese, Cagdas D Onal, and Daniela Rus. Autonomous Soft Robotic Fish Capable of Escape Maneuvers Using Fluidic Elastomer Actuators. *Soft robotics*, 1(1):75–87, 2014. 1

[14] Adam Paszke, Sam Gross, Francisco Massa, Adam Lerer, James Bradbury, Gregory Chanan, Trevor Killeen, Zeming Lin, Natalia Gimelshein, Luca Antiga, Alban Desmaison, Andreas Kopf, Edward Yang, Zachary DeVito, Martin Raison, Alykhan Tejani, Sasank Chilamkurthy, Benoit Steiner, Lu Fang, Junjie Bai, and Soumith Chintala. Pytorch: An imperative style, high-performance deep learning library. In *Advances in Neural Information Processing Systems 32*, pages 8024–8035. Curran Associates, Inc., 2019. 6

[15] Pietro Pustina, Pablo Borja, Cosimo Della Santina, and Alessandro De Luca. P-sati-d shape regulation of soft robots. *IEEE Robotics and Automation Letters*, 8(1): 1–8, 2022.

[16] Federico Renda, Frédéric Boyer, Jorge Dias, and Lakmal Seneviratne. Discrete cosserat approach for multisection soft manipulator dynamics. *IEEE Transactions on Robotics*, 34(6):1518–1533, 2018. 1, 3, 6

[17] José Guadalupe Romero, Romeo Ortega, and Ioannis Sarras. A globally exponentially stable tracking controller for mechanical systems using position feedback. *IEEE Transactions on Automatic Control*, 60(3):818–823, 2014. 2, 3

[18] Chia-Hsien Shih, Noel Naughton, Udit Halder, Heng-Sheng Chang, Seung Hyun Kim, Rhanor Gillette, Prashant G Mehta, and Mattia Gazzola. Hierarchical control and learning of a foraging cyberoctopus. *Advanced Intelligent Systems*, page 2300088, 2023. 2

[19] Jean-Jacques E ; Weiping Li Slotine. On the adaptive control of robot manipulators. *The International Journal of Robotics Research*, 6:49–59, 1987. doi: 10.1177/027836498700600303.

[20] Mark W Spong. Remarks on robot dynamics: Canonical transformations and riemannian geometry. pages 554–559. IEEE International Conference on Robotics and Automation, 5 1992.

[21] Mark W. Spong. An historical perspective on the control of robotic manipulators. *Annual Review of Control, Robotics, and Autonomous Systems*, 5:1–31, 2022. 6

[22] Mark W Spong and Mathukumalli Vidyasagar. *Robot Dynamics and Control*. John Wiley & Sons, 2008.

[23] Hong Kai Yap, Nazir Kamaldin, Jeong Hoon Lim,

Fatima A Nasrallah, James Cho Hong Goh, and Chen-Hua Yeow. A Magnetic Resonance Compatible Soft Wearable Robotic Glove for Hand Rehabilitation and Brain Imaging. *IEEE transactions on neural systems and rehabilitation engineering*, 25(6):782–793, 2016. 1